Supplementary information: The response of wildfire regimes to Last Glacial Maximum carbon dioxide and climate

Olivia Haas[1,2], Iain Colin Prentice[1,2], Sandy P. Harrison[1,3]

[1]Leverhulme Centre for Wildfires, Environment and Society, Imperial College London, South Kensington, London SW7 2BW, UK

[2]Georgina Mace Centre for the Living Planet, Department of Life Sciences, Imperial College London, Silwood Park Campus, Buckhurst Road, Ascot SL5 7PY, UK

[3]Geography & Environmental Science, University of Reading, Whiteknights, Reading RG6 6AH, UK

S1. Obtaining Fraction of Absorbed Photosynthetically Active Radiation (fAPAR) from BIOME4.

BIOME4 (Kaplan et al., 2003) is a coupled biogeography and biogeochemistry with which we can simulate the equilibrium distribution of biomes from latitude, atmospheric CO2 concentration, mean monthly precipitation, temperature, and cloud cover. On of the outputs provided by the model is monthly leaf area index (LAI), which we can convert to Fraction of Absorbed Photosynthetically Active Radiation (fAPAR) using Beer-Lamberth law:

$$fAPAR = 1 - \exp(-k.\ LAI) \qquad (2)$$

where k ≈ 0..5, a constant extinction coefficient (Saitoh et al., 2012).

fAPAR simulated from BIOME4 under modern-day conditions (2010-2015 seasonal climatology; Cucchi et al., 2020) overestimated fAPAR compared to observed fAPAR from NASA/GIMMS fAPAR 3g from the same period. As such, we rescaled the simulated BIOME fAPAR for each experiment such that:

$$fAPAR_{rescaled} = fAPAR_{exp} \frac{fAPAR_{obs}}{fAPAR_{sim}}) \qquad (3),$$

$where\ fAPAR_{rescaled}$ is the monthly rescaled fAPAR for that experiment, $fAPAR_{exp}$ is the original fAPAR output from BIOME4 for that experiment and $\frac{fAPAR_{obs}}{fAPAR_{sim}}$ is a constant scaling factor, determined for each biome, where $fAPAR_{obs}$ is the monthly NASA/GIMMS fAPAR 3g median value for that biome, and $fAPAR_{sim}$ is the monthly fAPAR median value simulated by BIOME4 for that biome. This method provided a rescaled fAPAR for the modern day that was correlated at 0.63 with the observational data, compared to 0.13 for the original BIOME4 fAPAR output for the same period, a reasonable estimation of fAPAR for each of the experiments.

S2. Obtaining burnt area mask for fire size and fire intensity experiments

In this analysis, we were interested in how the global pattern of burnt area (BA), fire size (FS) and fire intensity (FI) change under different climate and CO_2 scenarios. Both the GLM models for FS and FI return values of estimated FS and FI assuming a fire occurs since the models were fitted to observed data for FS and FI. When no fire occurred, there was no data for either FS or FI. As such, these models cannot determine themselves if an ignition occurred.

To study changes in FS and FI, it is necessary to apply an ignition threshold, which we obtained from the BA model. The burnt area (BA) generalized linear model (GLM) provides a robust reconstruction of BA under the model training conditions with a 0.8 correlation between the observational data and the fitted values(Haas et al., 2022). There are no systematic biases evident from plotting the residuals of the model but there is a compression of the range of reconstructed values, leading to apparent over- (under-) prediction at the low (high) extremes. This is to be expected, as the observational values reflect what really happened over the study period. Whilst some exceptionally large/intense wildfires occurred, many grid-cells also had no fire activity whilst the fitted values represent the probability of burning in each grid-cell, regardless of what happened during the study period. We obtained the ignition threshold value by studying the distribution of reconstructed BA values under the original model training period (2010-2015) when the observed BA value is 0, representing 26% of the grid-cells (a total of 14,816 data points and associated fitted values). We then took the median value of these fitted values as a threshold for ignition.

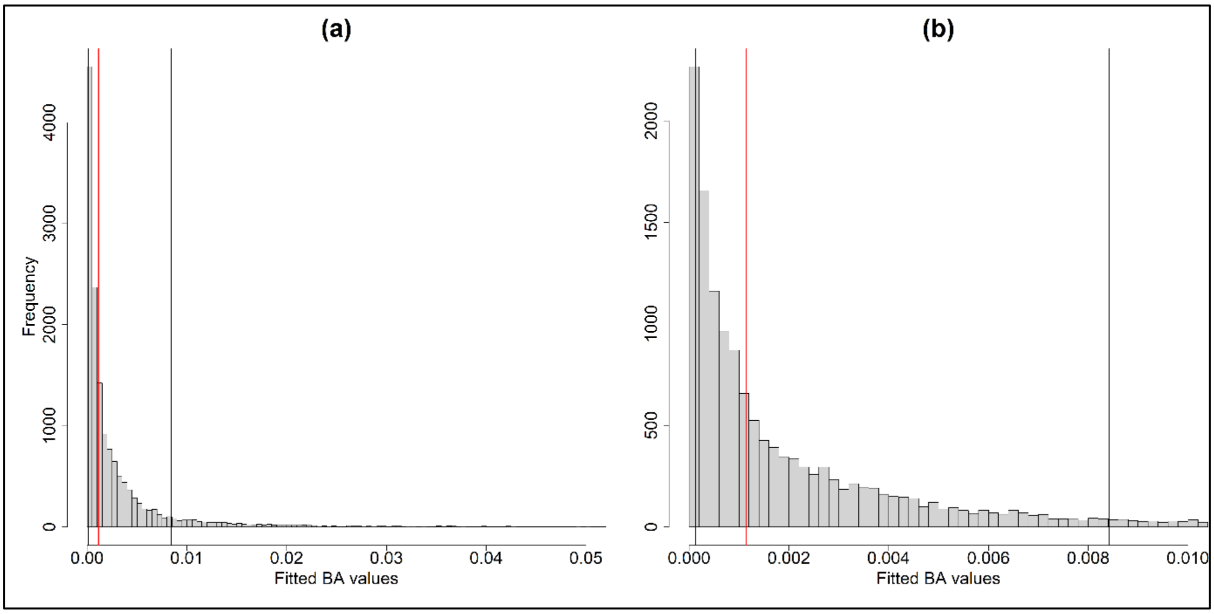

Figure S2.1. Histograms showing the distribution of the fitted values by the GLM BA model when observed BA values are 0 in the 2010-2015 climatology for (a) the whole range and (b) the range up to the 95th percentile. The red line shows the median value, and the black lines show the 10th and 90th percentile values.

	10th percentile	50th percentile	90th percentile
Fitted BA	0.0001	0.0011	0.0084

Table S1.1. Statistics for the fitted BA distribution when observed BA is 0 for the 2010-2015 climatology.

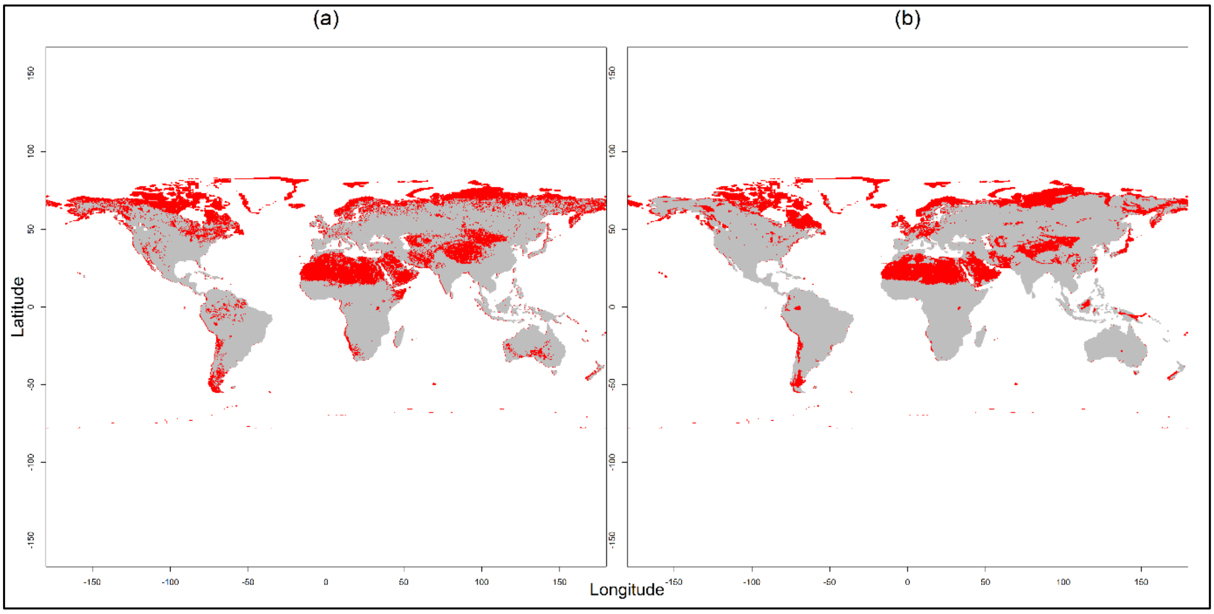

Figure S.2.2. Maps of BA ignition mask (where no burning is assumed to occur) under modern-day conditions (2010-2015 climatology) showing in red (a) where the observational BA values are 0 and (b) where the fitted BA values are equal or lower to 0.0011.

S3. Mapped results from the 12 experiments for all three LGM scenarios.

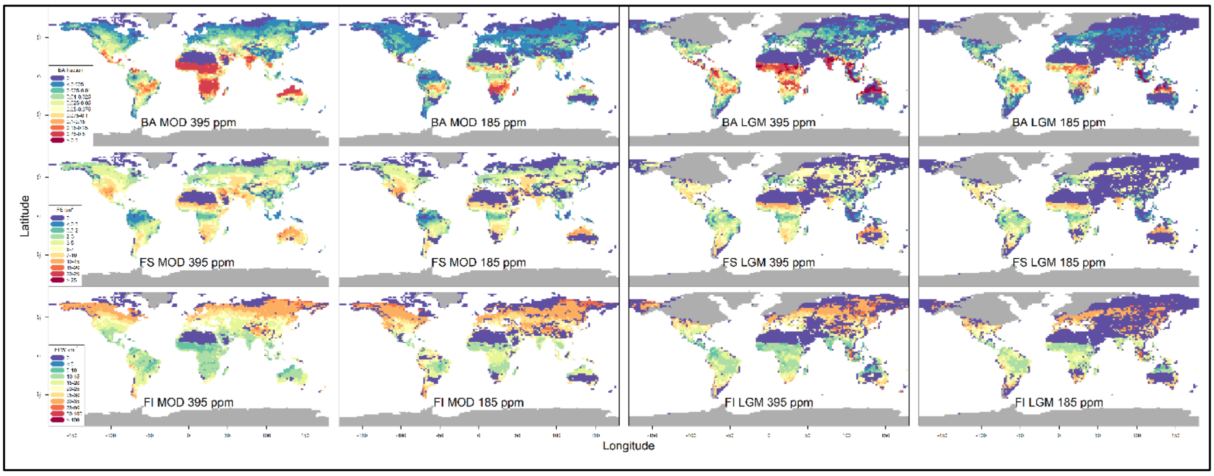

Figure S3.1. Changes in burnt area (BA), fire size (FS) and fire intensity (FI) using modern day climate (MOD) or Last Glacial Maximum (LGM) climate from the MPI-ESM1.2 simulation with either modern (395 ppm) or LGM (185 ppm) CO_2.

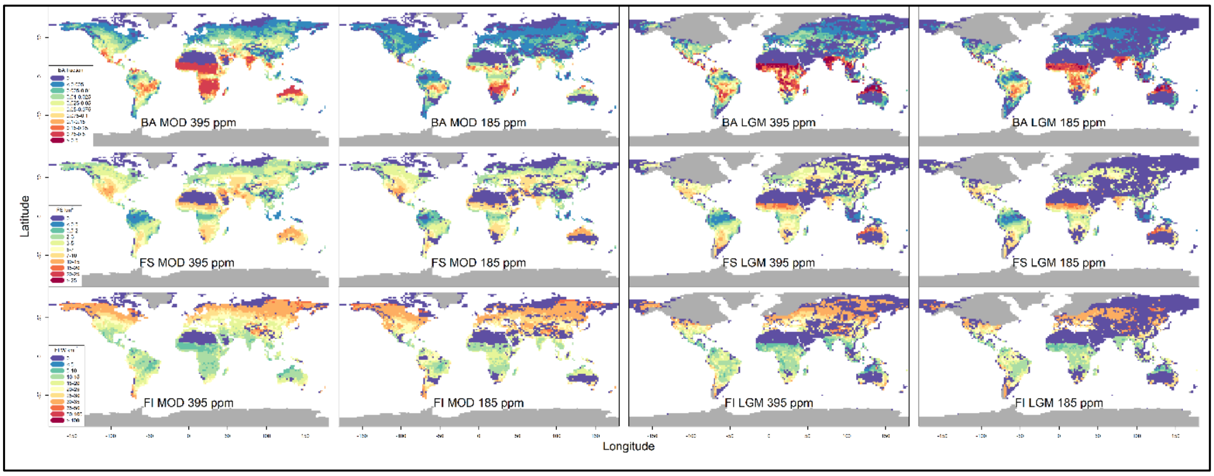

Figure S3.2. Changes in burnt area (BA), fire size (FS) and fire intensity (FI) using modern day climate (MOD) or Last Glacial Maximum (LGM) climate from the AWIESM1 simulation with either modern (395 ppm) or LGM (185 ppm) CO_2.

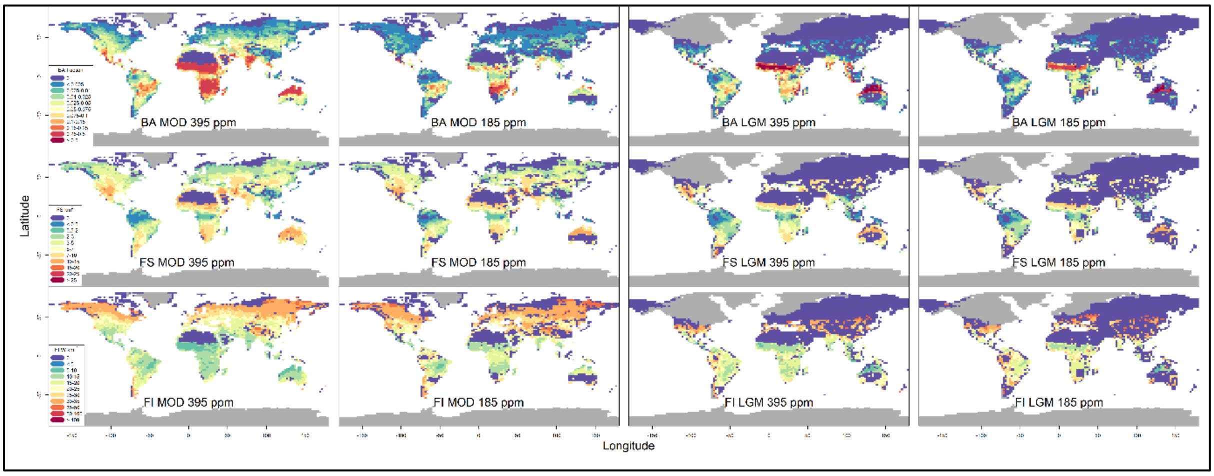

Figure S3.3. Changes in burnt area (BA), fire size (FS) and fire intensity (FI) using modern day climate (MOD) or Last Glacial Maximum (LGM) climate CESM1.2 simulation with either modern (395 ppm) or LGM (185 ppm) CO_2.

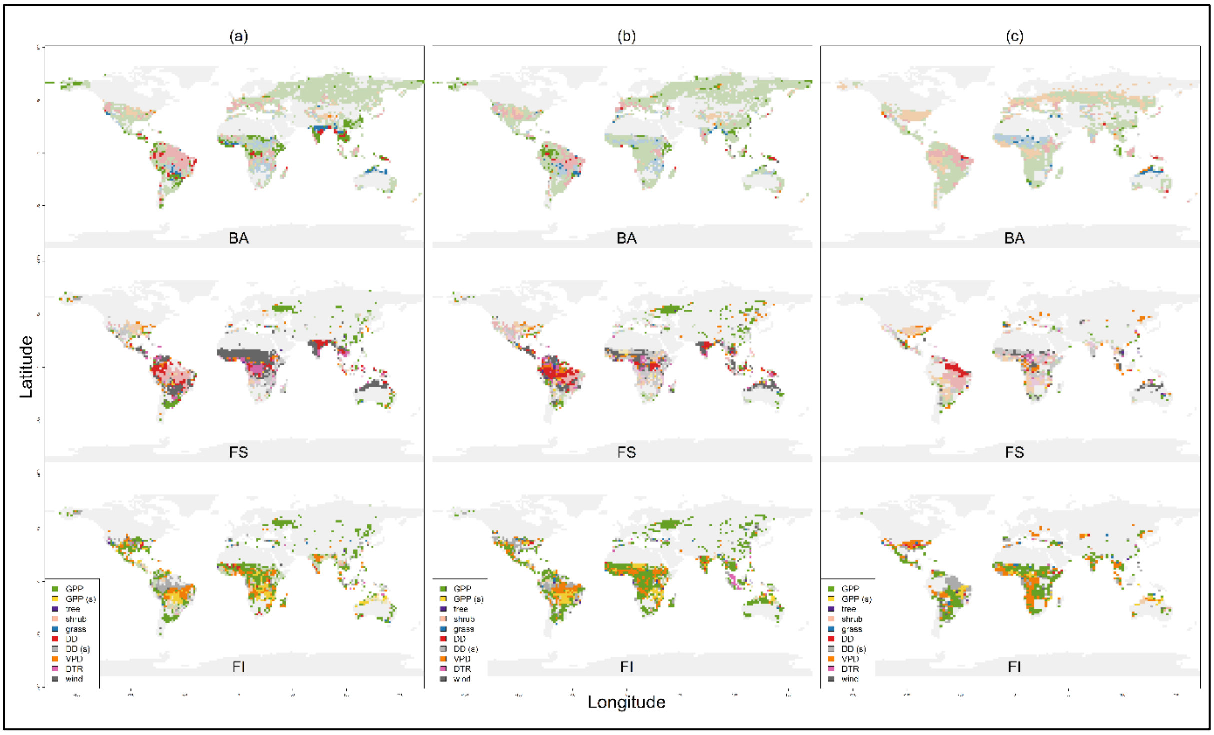

Figure S3.4. Map showing which model variable was responsible for some of the most important grid-cell changes between the realistic modern-day climate (MOD) 395 ppm experiment and the realistic Last Glacial Maximum (LGM) 190 ppm scenarios for BA, FS and FI for (a) the AWIESM1 LGM scenario, (b) the MPI-ESM1.2 LGM scenario and (c) the CESM1.2 LGM scenarios. Faded colors represent that the effect was a negative one, leading to a decrease in the wildfire property at the LGM whilst full colors represent an increase in the wildfire property at the LGM.

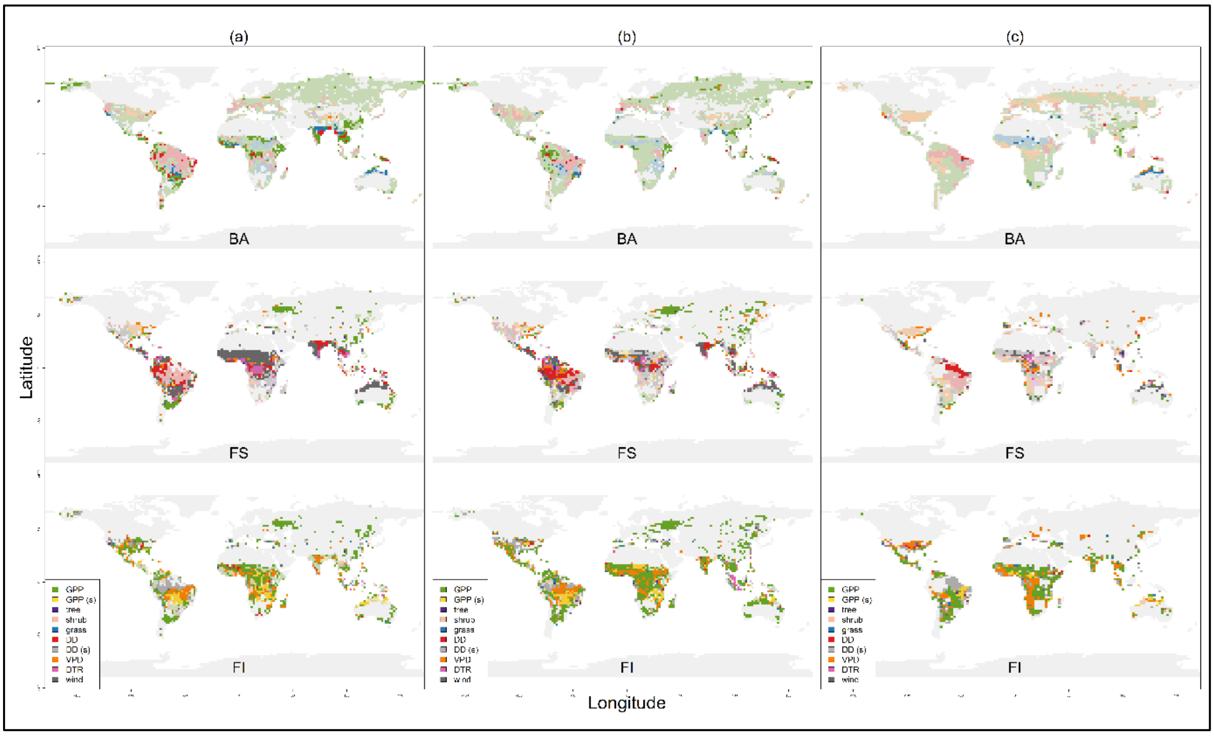

Figure S3.5. Map showing which model variable was responsible for some of the most important grid-cell changes between the MOD 395 ppm and LGM 395 ppm experiment (LGM climate/MOD CO_2) for BA, FS and FI for (a) the AWIESM1 LGM scenario, (b) the MPI-ESM1.2 LGM scenario and (c) the CESM1.2 LGM scenarios. Faded colors represent that the effect was a negative one, leading to a decrease in the wildfire property at the LGM whilst full colors represent an increase in the wildfire property at the LGM.

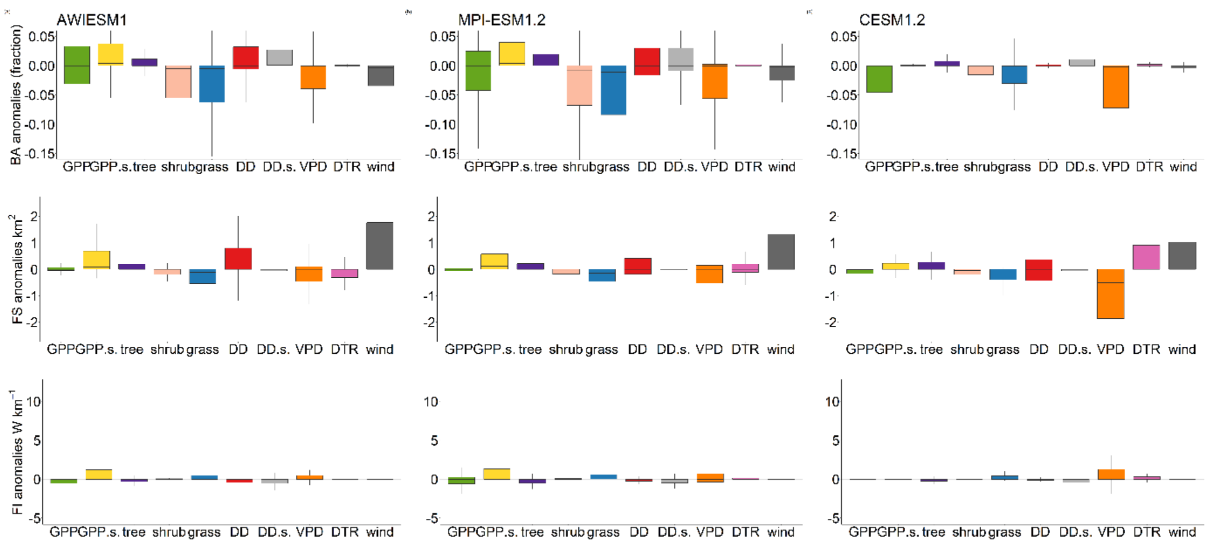

Figure S3.6. Boxplots showing relative importance of each predictor (GPP; gross primary production, GPP.s.; GPP seasonality, tree; tree cover, shrub; shrub cover, grass; grass cover, DD; dry days, DD.s.; dry days seasonality, VPD; vapour pressure deficit, DTR; diurnal temperature range, wind; wind speed) in driving the anomaly between the MOD 395 ppm and LGM 395 ppm experiment. For each grid cell common to both experiments (on modern-day continental shelves and masking the LGM ice sheets), the predictor which cause the largest change in the anomaly between the two experiments when it was excluded from the GLM model was retained, it is the change in anomaly that is shown here. This was taken as an indicator of relative importance of that predictor in driving the observed change for (a) the AWIESM1 LGM scenario, (b) the MPI-ESM-1.2 LGM scenario and (c) the CESM1.2 LGM scenario. A positive anomaly represents the variable driving an increase in BA, FS or FI at the LGM and a negative anomaly represents the variable driving a decrease in BA, FS or FI at the LGM.

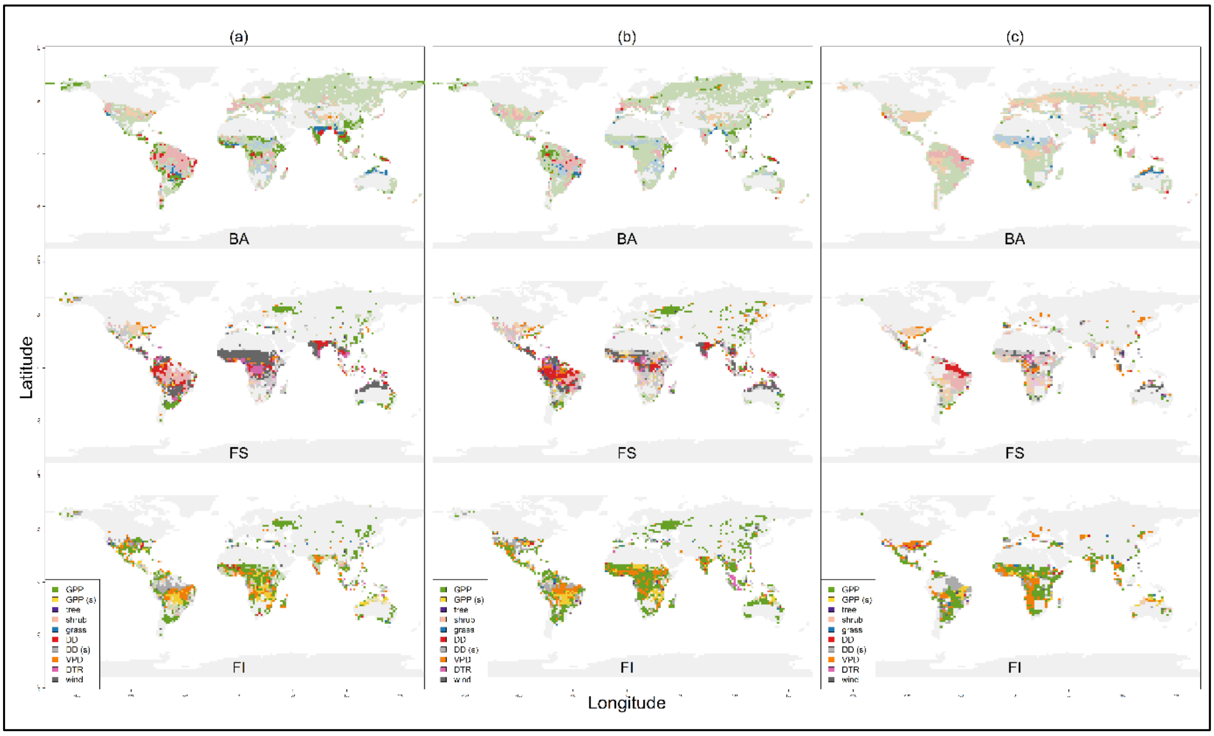

Figure S3.7. Map showing which model variable was responsible for some of the most important grid-cell changes between the realistic MOD 395 ppm and MOD 190 ppm experiment (MOD climate/LGM CO_2) for BA, FS and FI for (a) the AWIESM1 LGM scenario, (b) the MPI-ESM1.2 LGM scenario and (c) the CESM1.2 LGM scenarios. Faded colors represent that the effect was a negative one, leading to a decrease in the wildfire property at the LGM whilst full colors represent an increase in the wildfire property at the LGM.

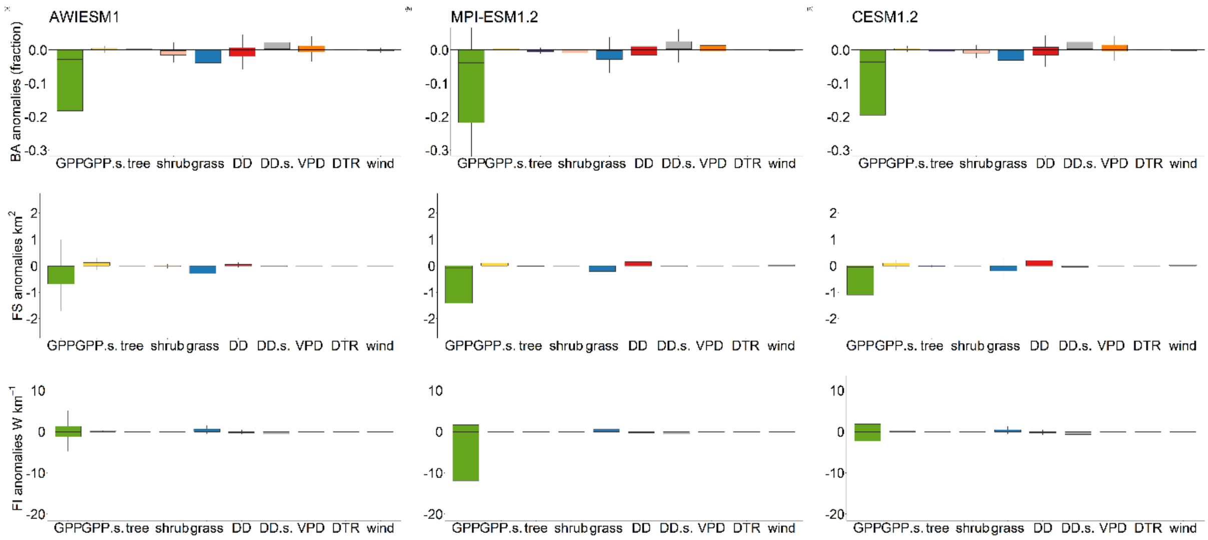

Figure S3.8. Boxplots showing relative importance of each predictor (GPP; gross primary production, GPP.s.; GPP seasonality, tree; tree cover, shrub; shrub cover, grass; grass cover, DD; dry days, DD.s.; dry days seasonality, VPD; vapour pressure deficit, DTR; diurnal temperature range, wind; wind speed) in driving the anomaly between the MOD 395 ppm and MOD 190 ppm experiment. For each grid cell common to both experiments (on modern-day continental shelves and masking the LGM ice sheets), the predictor which cause the largest change in the anomaly between the two experiments when it was excluded from the GLM model was retained, it is the change in anomaly that is shown here. This was taken as an indicator of relative importance of that predictor in driving the observed change for (a) the AWIESM1 LGM scenario, (b) the MPI-ESM-1.2 LGM scenario and (c) the CESM1.2 LGM scenario. A positive anomaly represents the variable driving an increase in BA, FS or FI at the LGM and a negative anomaly represents the variable driving a decrease in BA, FS or FI at the LGM.

S4. Comparison of experiments with charcoal records from the Reading Palaeofire Database (RPD)

BA experiments		MPI_ESM1.2			AWIESM1			CESM1.2 LGM		
Scenario	RPD	LGM 190	MOD 190	LGM 395	LGM 190	MOD 190	LGM 395	LGM 190	MOD 190	LGM 395
Negative RPD anomalies										
Number of records	35	20	21	13	17	21	10	20	20	17
Successful identification (percentage)		57	60	37	49	60	29	57	57	49
Positive RPD anomalies										
Number of records	16	3	0	8	6	0	5	0	0	3
Successful identification (percentage)		19	0	50	38	0	31	0	0	19
Total RPD anomalies										
Number of records	51	23	21	21	23	21	15	20	20	20
Successful identification (percentage)		45	41	41	45	41	29	39	39	39

Table S4.1. Comparison of sign in BA anomalies (between the MOD climate/MOD CO_2 experiment and other three experiments respectively) at the location of each RDP (Harrison et al., 2022) charcoal-based reconstructions record. A positive anomaly represents increased biomass burning, and a negative anomaly represents decrease biomass burning. A successful identification means that the sign of the experiment anomaly and the sign of the RPD charcoal-based reconstructions are the same.

FS experiments		MPI_ESM1.2			AWIESM1			CESM1.2 LGM		
Scenario	RPD	LGM 190	MOD 190	LGM 395	LGM 190	MOD 190	LGM 395	LGM 190	MOD 190	LGM 395
Negative RPD anomalies										
Number records showing reduced burning	35	10	15	7	11	9	8	10	14	11
Successful identification (percentage)		29	43	20	31	26	23	29	40	31
Positive RPD anomalies										
Number records showing increased burning	16	6	2	7	8	8	9	4	2	4
Successful identification (percentage)		38	13	44	50	50	56	25	13	25
Total RPD anomalies										
Total number of records	51	16	17	14	19	17	17	14	16	15
Successful identification (percentage)		31	33	27	37	33	33	27	31	29

Table S4.2. Comparison of sign in FS anomalies (between the MOD climate/MOD CO_2 experiment and other three experiments respectively) at the location of each RDP (Harrison et al., 2022) charcoal-based reconstructions record. A positive anomaly represents increased biomass burning, and a negative anomaly represents decrease biomass burning. A successful identification means that the sign of the experiment anomaly and the sign of the RPD charcoal-based reconstructions are the same.

FI experiments		MPI_ESM1.2			AWIESM1			CESM1.2 LGM		
Scenario	RPD	LGM 190	MOD 190	LGM 395	LGM 190	MOD 190	LGM 395	LGM 190	MOD 190	LGM 395
Negative RPD anomalies										
Number records showing reduced burning	35	5	7	9	7	7	11	3	5	4
Successful identification (percentage)		14	20	26	20	20	31	9	14	11
Positive RPD anomalies										
Number records showing increased burning	16	10	12	7	10	12	8	9	11	8
Successful identification (percentage)		63	75	44	63	75	50	56	69	50
Total RPD anomalies										
Total number of records	51	15	19	16	17	19	19	12	16	12
Successful identification (percentage)		30	37	31	33	37	37	24	31	24

Table S4.3. Comparison of sign in FI anomalies (between the MOD climate/MOD CO_2 experiment and other three experiments respectively) at the location of each RDP (Harrison et al., 2022) charcoal-based reconstructions record. A positive anomaly represents increased biomass burning, and a negative anomaly represents decrease biomass burning. A successful identification means that the sign of the experiment anomaly and the sign of the RPD charcoal-based reconstructions are the same.

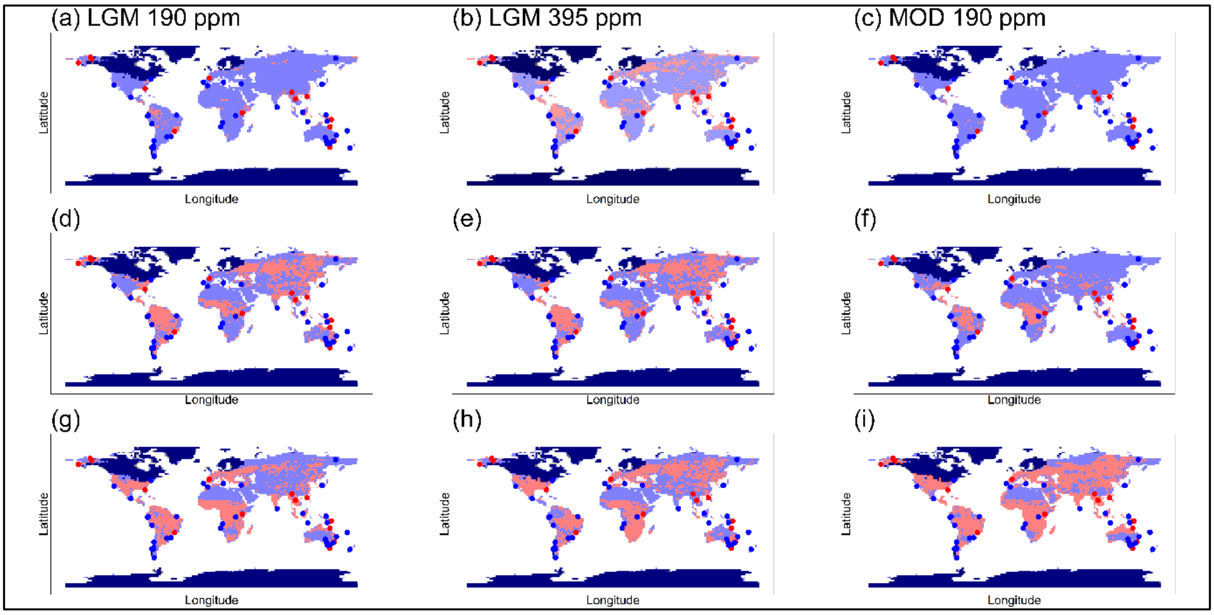

Figure S4.1 Comparison of anomalies between the experiment outputs from the MPI-ESM1.2 LGM scenario with charcoal records from the Reading Palaeofire Database (RPD) for (a) the relatistic BA LGM experiment (b) the BA LGM climate/MOD CO_2 sensitivity experiment and (c) the BA MOD climate/LGM CO_2 sensitivity experiment (d) the relatistic FS LGM experiment (e) the FS LGM climate/MOD CO_2 sensitivity experiment and (f) the FS MOD, (g) the relatistic FI LGM experiment (h) the FI LGM climate/MOD CO_2 sensitivity experiment and (i) the FI MOD climate/LGM CO_2 sensitivity experiment climate/LGM CO_2 sensitivity experiment. The modeled positive LGM-MOD anomalies are shown in red and LGM-MOD negative anomalies in blue. Dotted red (positive anomaly) and blue (negative anomaly) points show the location of the RPD records for the LGM. The LGM ice sheets are shown in dark blue.

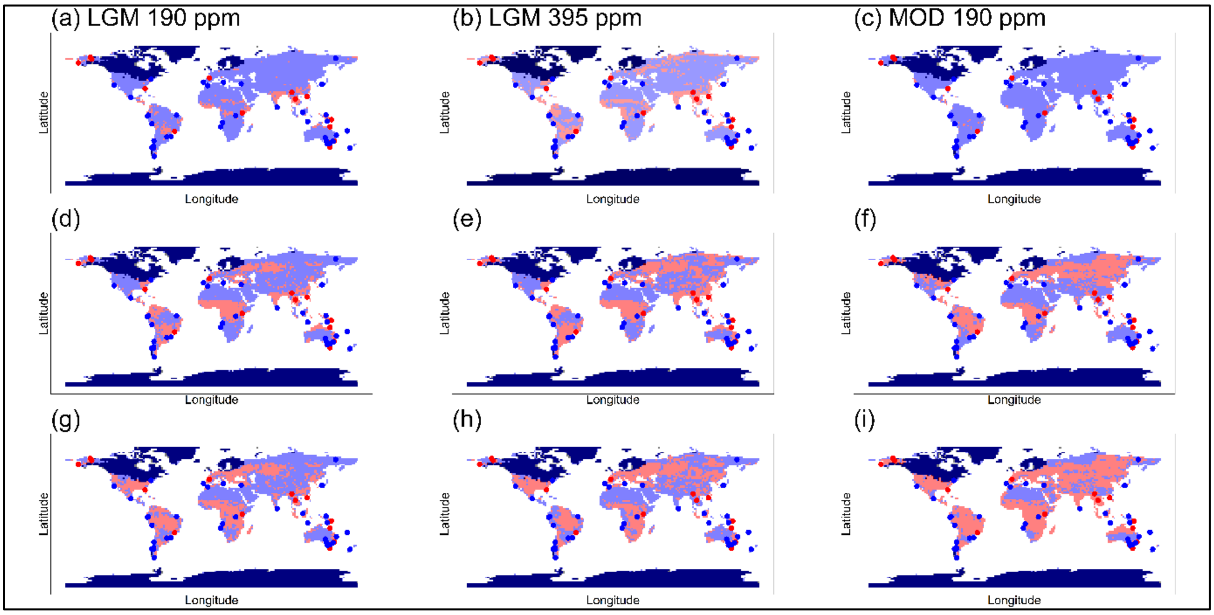

Figure S4.2 Comparison of anomalies between the experiment outputs from the AWIESM1 LGM scenario with charcoal records from the Reading Palaeofire Database (RPD) for (a) the relatistic BA LGM experiment (b) the BA LGM climate/MOD CO_2 sensitivity experiment and (c) the BA MOD climate/LGM CO_2 sensitivity experiment (d) the relatistic FS LGM experiment (e) the FS LGM climate/MOD CO_2 sensitivity experiment and (f) the FS MOD, (g) the relatistic FI LGM experiment (h) the FI LGM climate/MOD CO_2 sensitivity experiment and (i) the FI MOD climate/LGM CO_2 sensitivity experiment climate/LGM CO_2 sensitivity experiment. The modeled positive LGM-MOD anomalies are shown in red and LGM-MOD negative anomalies in blue. Dotted red (positive anomaly) and blue (negative anomaly) points show the location of the RPD records for the LGM. The LGM ice sheets are shown in dark blue.

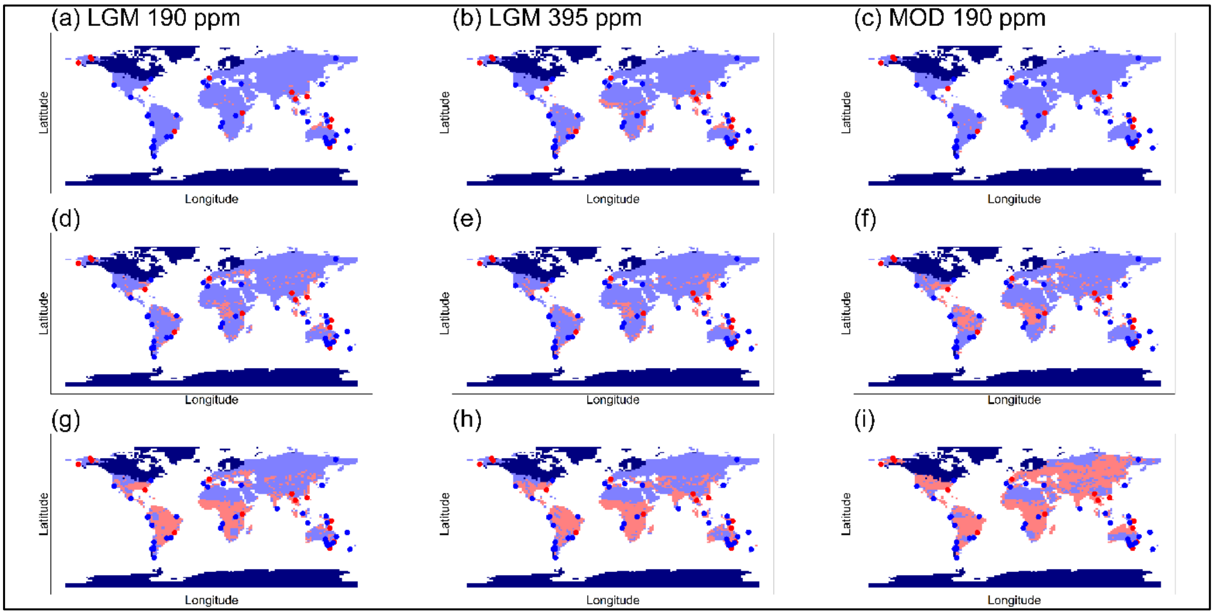

Figure S4.3 Comparison of anomalies between the experiment outputs from the CESM1.2 LGM scenario with charcoal records from the Reading Palaeofire Database (RPD) for (a) the relatistic BA LGM experiment (b) the BA LGM climate/MOD CO_2 sensitivity experiment and (c) the BA MOD climate/LGM CO_2 sensitivity experiment (d) the relatistic FS LGM experiment (e) the FS LGM climate/MOD CO_2 sensitivity experiment and (f) the FS MOD, (g) the relatistic FI LGM experiment (h) the FI LGM climate/MOD CO_2 sensitivity experiment and (i) the FI MOD climate/LGM CO_2 sensitivity experiment climate/LGM CO_2 sensitivity experiment. The modeled positive LGM-MOD anomalies are shown in red and LGM-MOD negative anomalies in blue. Dotted red (positive anomaly) and blue (negative anomaly) points show the location of the RPD records for the LGM. The LGM ice sheets are shown in dark blue.

References

Cucchi, M., Weedon, G. P., Amici, A., Bellouin, N., Lange, S., Müller Schmied, H., Hersbach, H., & Buontempo, C. (2020). WFDE5: bias-adjusted ERA5 reanalysis data for impact studies. *Earth System Science Data*, *12*(3), 2097–2120.

Haas, O., Prentice, I. C., & Harrison, S. P. (2022). Global environmental controls on wildfire burnt area, size, and intensity. *Environmental Research Letters*, *17*(6), 065004.

Harrison, S.P., Villegas-Diaz, R., Cruz-Silva, E., Gallagher, D., Kesner, D., Lincoln, P., Shen, Y., Sweeney, L., Colombaroli, D., Ali, A., Barhoumi, C., Bergeron, Y., Blyakharchuk, T., Bobek, P., Bradshaw, R., Clear, J.L., Czerwiński, S., Daniau, A-L., Dodson, J., Edwards, K.J., Edwards, M.E., Feurdean, A., Foster, D., Gajewski, K., Gałka, M., Garneau, M., Giesecke, T., Gil Romera, G., Girardin, M.P., Hoefer, D., Huang, K., Inoue, J., Jamrichová, E., Jasiunas, N., Jiang, W., Jiménez-Moreno, G., Karpińska-Kołaczek, M., Kołaczek, P., Kuosmanen, N., Lamentowicz, M., Lavoie, M., Li, F., Li, J., Lisitsyna, O., López-Sáez, J.A., Luelmo-Lautenschlaeger, R., Magnan, G., Magyari, E.K., Maksims, A., Marcisz, K., Marinova, E., Marlon, J., Mensing, S., Miroslaw-Grabowska, J., Oswald, W., Pérez-Díaz, S., Pérez-Obiol, R., Piilo, S., Poska, A., Qin, X., Remy, C.C., Richard, P.J.H., Salonen, S., Sasaki, N., Schneider, H., Shotyk, W., Stancikaite, M., Šteinberga, D., Stivrins, N., Takahara, H., Tan, Z., Trasune, L., Umbanhowar, C.E., Väliranta, M., Vassiljev, J., Xiao, X., Xu, Q., Xu, X., Zawisza, E., Zhao, Y., Zhou, Z., & Paillard, J. (2022). The Reading Palaeofire database: an expanded global resource to document changes in fire regimes from sedimentary charcoal records *Earth System Science Data* 14: 1109-1124 https://doi.org/10.5194/essd-14-1109-2022

Kaplan, J.O., Bigelow, Prentice, I.C., Harrison, S.P., P.J., N.H., Bartlein, Christensen, T.R., Cramer, W., Matveyeva, N.V., McGuire, A.D., Murray, D.F., Razzhivin, V.Y., Smith, B. and Walker, D.A., Anderson, P.M., Andreev, A.A., Brubaker, L.B., Edwards, M.E., & Lozhkin, A.V. (2003). Climate change and Arctic ecosystems II: Modeling, palaeodata-model comparisons, and future projections. *Journal of Geophysical Research-Atmosphere* 108, No. D19, 8171. (DOI: 10.1029/2002JD002559).

Saitoh, T. M., Nagai, S., Noda, H. M., Muraoka, H., & Nasahara, K. N. (2012). Examination of the extinction coefficient in the Beer–Lambert law for an accurate estimation of the forest canopy leaf area index. *Forest Science and Technology*, *8*(2), 67–76.